

FATIGUE LIFE EXTENSION OF STEAM TURBINE ALLOYS USING LOW PLASTICITY BURNISHING (LPB)

Paul S. Prevéy
Lambda Research, Inc.
Cincinnati, OH, USA

Dr. Nayarananan Jayaraman
Lambda Research, Inc.
Cincinnati, OH, USA

Ravi Ravindranath
NAVAIR
Patuxent River, MD, USA

ABSTRACT

Low Plasticity Burnishing (LPB) dramatically improves the damage tolerance of titanium alloy blades, mitigating blade-disk dovetail fretting and blade edge damage in gas turbines. LPB surface treatment of martensitic stainless steels Alloy 450 and 17-4PH subject to corrosion fatigue and pitting in the low-pressure sections of steam turbines has now been investigated. Condensation in the low-pressure steam turbine environment supports corrosion pitting and corrosion fatigue in martensitic stainless steels, primary failure mechanisms driving steam turbine repair and operational expense.

Chloride corrosion fatigue results with and without high k_f surface damage are compared for LPB, shot peened, and machined 17-4PH; and for ground and LPB treated Alloy 450. The depth and magnitude of compression achieved by the surface treatments are documented. LPB increased the undamaged fatigue strength of 17-4PH by 30% in neutral salt solution, and of Alloy 450 in acidic salt by 50%. In both alloys LPB mitigated damage to the 1 mm depth of compression. The cyclic stress corrosion component of corrosion fatigue was eliminated by the deep LPB compression, effectively restoring the endurance limit lost in active corrosion fatigue in both alloys.

Keywords: Residual Stresses, Surface Enhancement, Corrosion Fatigue, High Cycle Fatigue (HCF), Low Plasticity Burnishing (LPB), Shot Peening (SP), Foreign Object Damage (FOD)

INTRODUCTION

A surface layer of beneficial residual compressive stresses in metallic components has long been recognized¹⁻⁴ to enhance fatigue strength. Shot peening is widely used in the automotive and aerospace industries, including gas and steam turbines. Low plasticity burnishing (LPB)⁵, laser shock peening (LSP)⁶, and ultrasonic peening⁷ have emerged that can produce deeper compression with much less cold working of the surface than shot peening. Reduced cold working improves the thermal and mechanical stability of the beneficial compression in service.⁸

Corrosion fatigue, stress corrosion cracking, and fatigue initiated from corrosion and erosion pits are the primary degradation processes that affect low pressure steam turbine components manufactured from stainless steels.⁹⁻¹² Two martensitic alloys widely used where a combination of high strength and resistance to corrosion are required were chosen for study: the precipitation hardened 17-4PH and age-hardenable Alloy 450.

Low plasticity burnishing (LPB) has been demonstrated to provide a deep surface layer of high magnitude compression in aluminum, titanium, nickel alloys and steels to mitigate fatigue damage mechanisms including foreign object damage (FOD),¹³⁻¹⁵ fretting,¹⁶⁻¹⁷ and corrosion fatigue.¹⁸⁻²¹ The LPB process is performed on conventional CNC machine tools and robots at costs and speeds comparable to conventional machining.

Corrosion fatigue and stress corrosion cracking (SCC) research has generally focused on alloy chemistry, microstructure control, and chemical modification or coating of the surface. The current study investigates the use of the layer of compressive residual stress imparted by LPB to mechanically suppress local stress concentrations and the cyclic SCC component of corrosion fatigue to improve the performance of martensitic stainless steels.

EXPERIMENTAL PROCEDURE

Material and Heat Treatment

17-4 PH stainless steel was procured in the form of 0.5 in. (~12.7 mm) thick plates. Bars of nominal dimensions of 0.375 in. X 1.25 in. X 8 in. (9.5 mm X 31.75 mm X 203.2 mm) were initially machined. All the bars were heat-treated to the H1100 condition: aged at 593 °C (1100 °F) for 4 hours and air-cooled.

17-4 PH Composition (wt%): C-0.040%, Nb-0.32%, Cr-15.35%, Cu-3.39%, Mn-0.69%, Mo-0.24%, Ni-4.24%, P-0.024%, S-0.006%, Si-0.63%, Ti-<0.01%, Bal-Fe.

17-4 PH Properties: 0.2% Y.S. = 156 ksi (~1,075 MPa), UTS = 160 ksi (~1,100 MPa), Elong. = 16%, RA = 66.4%

Alloy 450 stainless steel was procured in the form of forged bars of nominally 1.5 in. X 2 in. X 9 in. (38 mm X 50 mm X 225 mm). All bars were heat treated to the H1050 condition: solution treated at 1038 °C for 1 hour, water quench, aged at 566 °C for 4 hours, and air-cooled.

Alloy 450 Composition (wt%): C-0.029%, Nb-0.72%, Cr-14.95%, Cu-1.73%, Mn-0.43%, Mo-0.79%, Ni-7.06%, P-0.019%, S-0.002%, Si-0.45%, Ti-<0.01%, Bal-Fe.

Alloy 450 Properties: 0.2% Y.S. = 155 ksi (1,070 MPa), UTS = 166 ksi (1,145 MPa), % Elong. = 18.8, %RA = 68.6

Fatigue Specimen Processing

Thick section fatigue specimens with a trapezoidal cross section in the gauge section designed to force fatigue failures to initiate in the compressive gage section surface under 4-point bend loading were finish machined by low stress grinding (LSG).

To simulate surface damage from any source (handling, FOD, corrosion pitting or erosion), a semi-elliptical surface notch of depth of $a_o = 0.01$ in. (0.25 mm) and surface length of $2c_o = 0.06$ in. (1.5 mm) was introduced by electrical discharge machining (EDM). EDM leaves a cracked recast layer in residual tension at the bottom of the notch, producing a large fatigue debit with a k_f of nominally 5. EDM notching is

widely used for reproducible laboratory simulation of high k_f damage.

Surface Treatments

LPB process parameters were developed for both alloys to impart a depth and magnitude of compression on the order of 1mm, sufficient to mitigate the simulated FOD with minimal cold work. Figure 1 shows fatigue specimens in the process of being low plasticity burnished in the four-axis manipulator on the CNC milling machine.

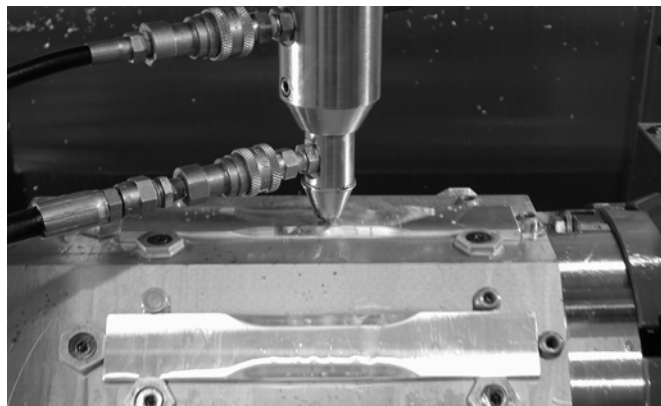


Figure 1: A set of 8 fatigue specimens being LPB processed in a 4-axis CNC milling machine.

Conventional air-blast shot peening was performed using 14CW (cut wire) shot, a rotating table, 125% coverage, to an 8A Almen intensity.

Corrosion Fatigue Testing

All fatigue tests were performed under constant amplitude loading on a Sonntag SF-1U fatigue machine in four-point bending. Fatigue testing was conducted at ambient temperature (~72F), a cyclic frequency of 30 Hz, and stress ratio, $R = S_{min}/S_{max} = 0.1$. Tests were conducted until specimen fracture or "run-out" life of 2.5×10^6 cycles. Run-out specimens were subsequently re-tested to fracture at a minimum stress at least 20 ksi greater than the stress level of initial run-out. Such re-tests results were regarded as valid and were included in S-N curves.

Active corrosion fatigue tests were carried out in an aqueous 3.5 wt% NaCl neutral salt solution for the 17-4PH and acidic (pH=3.5) for the Alloy 450. The pH of the solution was adjusted by adding either NaOH or HCl. At the start of cyclic loading, filter papers soaked with the solution were wrapped around the gage section of the fatigue test specimen and sealed with a polyethylene film to avoid evaporation. There was no exposure to the corrosive solution prior to the initiation of the fatigue tests.

For 17-4PH, LSG and LPB specimens were tested in air and in neutral NaCl solution, with and without EDM notch damage. SP specimens were tested only in air, with and without damage. A few LPB specimens were tested with EDM notches 2x and 3x deeper determine the limiting capability of the LPB treatment to withstand deeper damage.

Only LPB and LSF baseline samples of Alloy 450 were tested with and without EDM damage, all in acidic salt solution. A few Alloy 450 LPB samples were also tested with 2x and 3x deeper damage.

Residual Stress Measurement

X-ray diffraction residual stress measurements were made at the surface and below the surface to determine the depth and magnitude of residual stress distributions produced by the surface treatments. Measurements were made in the longitudinal direction of fatigue loading in the fatigue specimen gage employing a $\sin^2\psi$ technique and the diffraction of chromium $K\alpha_1$ radiation from the (211) planes of steel. The lattice spacing was first verified to be a linear function of $\sin^2\psi$, as required for the plane stress linear elastic residual stress model²²⁻²⁵.

Material was removed electrolytically for subsurface measurement in order to minimize possible alteration of the subsurface residual stress distribution as a result of material removal. The residual stress measurements were corrected for both the penetration of the radiation into the subsurface stress gradient²⁶ and for stress relaxation caused by layer removal.²⁷

The value of the x-ray elastic constants required to calculate the macroscopic residual stress from the strain normal to the (211) planes of steel were determined in accordance with ASTM E1426-9. Systematic errors were monitored per ASTM specification E915.

The $K\alpha_1$ peak breadth was calculated from the Pearson VII function fit used for peak location during macroscopic stress measurement.²⁸ The percent cold work was calculated using an empirical relationship established between the material cold working (true plastic strain) and the $K\alpha_1$ line broadening.²⁹ The percent cold work is a scalar quantity, taken to be the true plastic strain necessary to produce the diffraction peak width measured based on the empirical relationship. Because cold work calibration data was obtained only for 17-4PH, subsurface cold work distributions are not reported for Alloy 450.

Fractography

Following fatigue testing, each specimen fracture face was examined optically at magnifications up to 60x to identify fatigue origins relative to the specimen geometry. Photographs were taken with a Nikon 990 digital camera through a Nikon Stereoscopic microscope at 15x. A representative photograph of a typical failure for each specimen group was obtained. A few selected specimens were also examined under a Cambridge S90B SEM.

RESULTS AND DISCUSSION

Residual Stress Distributions

The residual stress distributions measured as functions of depth are presented graphically in Figure 2 for the 17-4PH and in Figure 3 for the Alloy 450. Compressive stresses are shown as negative values, tensile as positive, in units of ksi (10^3 psi) and MPa (10^6 N/m²).

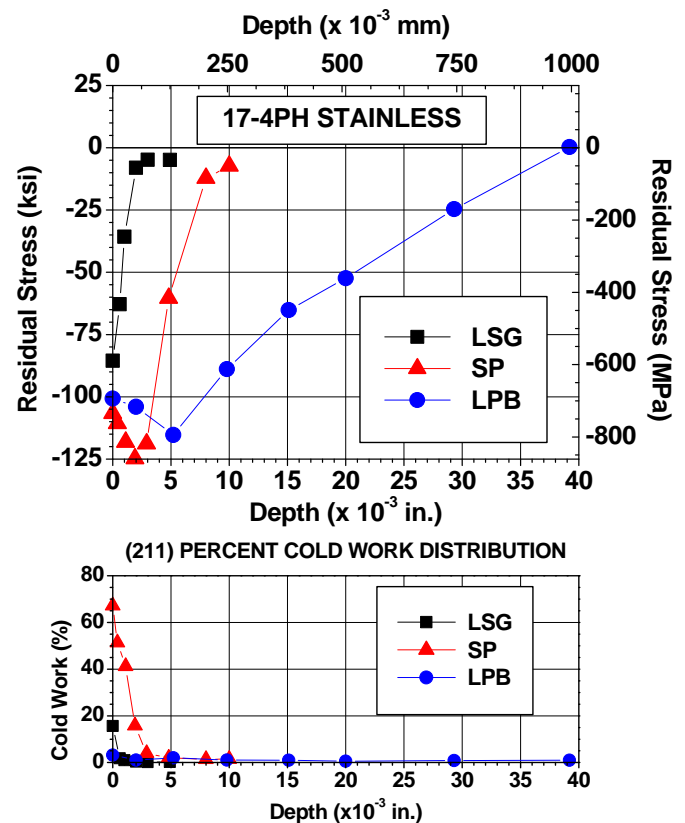


Figure 2. 17-4PH Residual stress distributions for LSG, SP and LPB, measured after fatigue testing.

Figure 2 shows the residual stress (RS) and cold work (CW) profiles for LSG, SP and LPB 17-4PH specimens after fatigue testing. LSG produces a thin layer of high compression, nominally -85 ksi (~-585 MPa), with 15% cold work at the surface, decreasing rapidly to nearly zero at a depth of 0.002 in. (~0.05 mm). SP produces higher surface compression of about -105 ksi (~-725 MPa), with nominally 70% cold work. Maximum compression of -125 ksi (~-860 MPa) occurs at a depth of about 0.002 in. (~0.05 mm), declining rapidly to nearly zero residual stress at a depth of about 0.010 in. (~0.25 mm). LPB produces surface compression of -100 ksi (~-690 MPa), maximum subsurface compressive of -115 ksi (~-790 MPa) at 0.005 in. (~0.125 mm), and gradually decreases to zero at a depth of about 0.040 in. (~1 mm). LPB produces surface cold work of < 5%, which decreases to nearly zero within 0.001 in. (~0.025 mm).

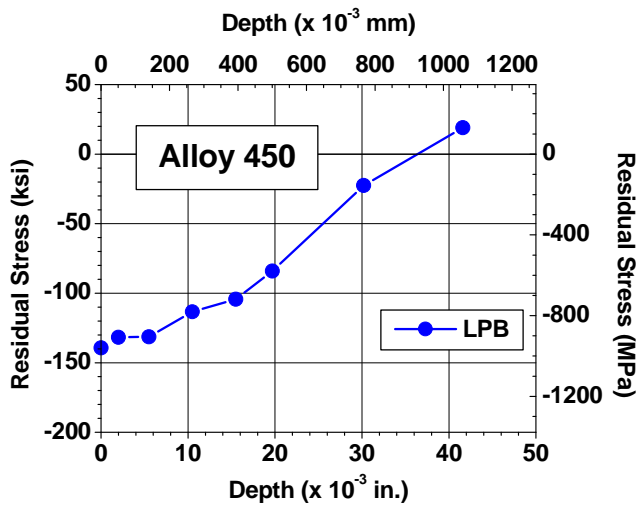


Figure 3. Alloy 450 Residual stress distribution for LPB processing

The residual stress (RS) profiles for LPB processed Alloy 450 after fatigue testing are shown in Figure 3. Maximum compression is nominally -140 ksi (-965 MPa) at the surface, decreasing to zero over a depth of about 0.035 in. (~0.9 mm) from the surface. The depth and magnitude of compression from LPB is comparable to the 17-4PH.

Measurement after failure of the samples in fatigue confirms that the beneficial residual compression in both alloys survives cyclic loading at stress levels much higher than typical service. The 17-4PH LPB sample failed after 200,000 cycles at a maximum stress of 210 ksi (1450 MPa). The Alloy 450 sample failed in 141,000 cycles, at 195 ksi (1345 MPa).

17-4PH Damage Tolerance and Corrosion Fatigue Performance

Figures 4 through 6 are S-N curves showing the fatigue performance with and without EDM notch damage and active corrosion during fatigue cycling of 17-4PH. Power law curves fitted to the baseline S-N data in Figure 4 are included in Figures 5 and 6 for comparison with the SP and LPB surface treatments.

The baseline low stress ground (LSG) results are presented in Figure 4. The fatigue strength of the unnotched (smooth) LSG condition at 10⁷ cycles was nominally 150 ksi (~1035 MPa). The fracture surface of a LSG specimen indicated multiple surface crack initiation sites. Exposure to active salt corrosion during fatigue cycling drops the fatigue strength to about 100 ksi (~690 MPa).

Introduction of the 0.010 in. (0.25 mm) deep EDM notch drastically decreases the fatigue strength to only 20 ksi (~140 MPa) for both air and salt corrosion environments. The fatigue lives with surface damage are over an order of magnitude shorter than the smooth baseline.

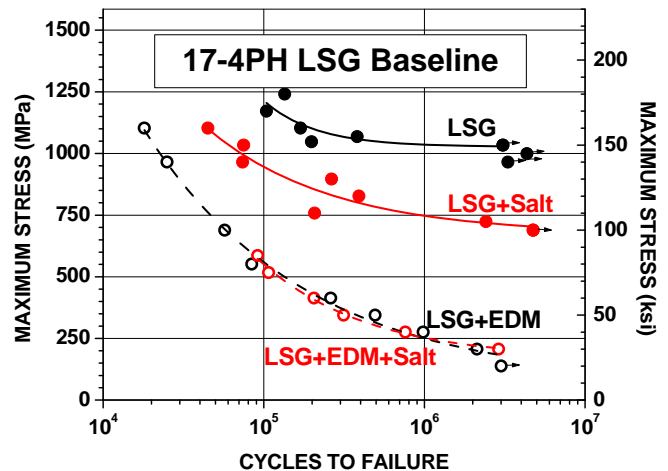


Figure 4. 17-4PH Baseline surface damage and corrosion fatigue results.

Figure 5 shows the fatigue performance of both smooth and notched SP treated specimens compared to the baseline data. No significant benefit is seen for SP over the LSG baseline condition. LSG is well known to produce a shallow surface layer of fairly high compression, typical of cold surface abrasion. Evidently, the difference in the depth and magnitude of the LSG and SP compressive layers, seen in Figure 2, is not sufficient to cause significantly different fatigue initiation and small crack growth. A small benefit in strength and life is evident for SP over LSG with EDM damage, attributed to the slightly deeper compressive layer from SP. Because SP provided only marginal

improvement over the LSG baseline condition, active corrosion fatigue testing was not performed for SP samples.

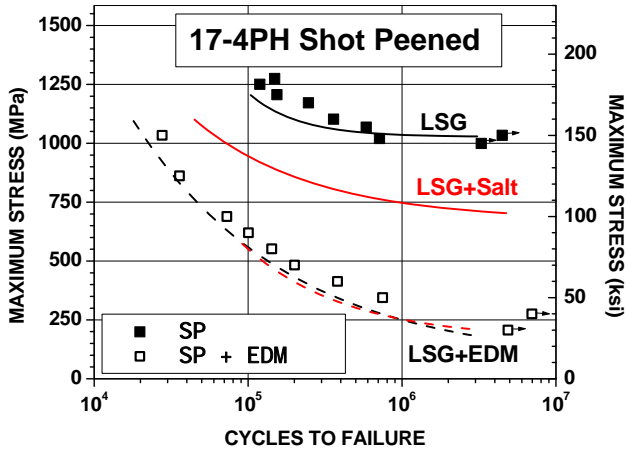


Figure 5. 17-4PH SP surface damage and corrosion fatigue results compared to Baseline. (Corrosion fatigue tests were not performed as noted in the text.)

The fatigue results for the LPB treated samples are shown in Figure 6 both with EDM damage and active corrosion during testing compared to the baseline curves. The fatigue strength of unnotched (smooth) LPB is significantly higher than SP, at nominally 190 ksi (~1310 MPa). All of the other LPB test conditions, including EDM notched, and corrosion fatigue with or without notches, are grouped together, indicating that the depth and magnitude of compression from LPB has mitigated the effects of active corrosion and the 0.010 in. deep damage. The fatigue strength of the LPB treated 17-4PH samples with damage and/or corrosion is nominally equivalent to the unnotched baseline LSG condition. The effect of corrosion during fatigue cycling, essentially cyclic stress corrosion cracking, is mitigated by LPB, effectively restoring the endurance limit typically lost in corrosion fatigue.

The ability of LPB to mitigate deeper damage was investigated. The fatigue strengths at 10^7 cycles for EDM notches up to 0.040 in. (1mm) deep are summarized in Figure 7. The SP and LSG performance to a depth of 0.010 in. (0.25 mm) is shown for comparison. The LPB treated specimens withstood even a 0.040 in. (~1 mm) deep EDM notch with a fatigue strength of at least 55 ksi (~380 MPa), roughly half of the baseline fatigue strength. For LSG and shot peened specimens a notch of 0.010 in depth resulted in dramatic loss of fatigue strength, to only 20% of baseline. Even with 0.040 in. deep damage, LPB retains 50% of the baseline strength, more than typical design strength for surface damage.

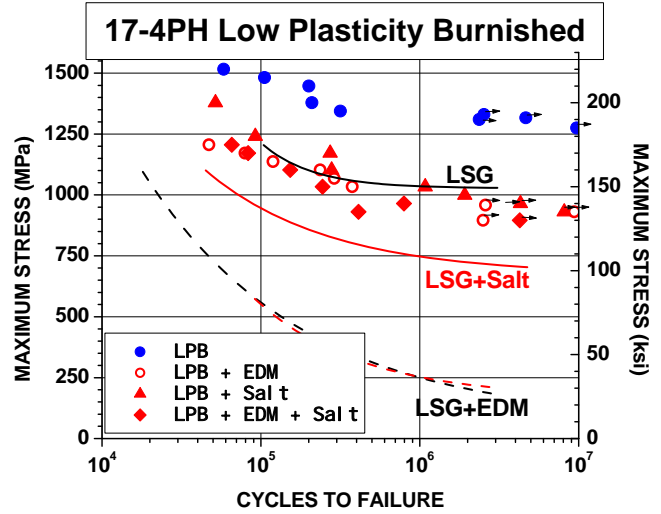


Figure 6. 17-4PH fatigue results for LPB treatment compared to the LSG baseline.

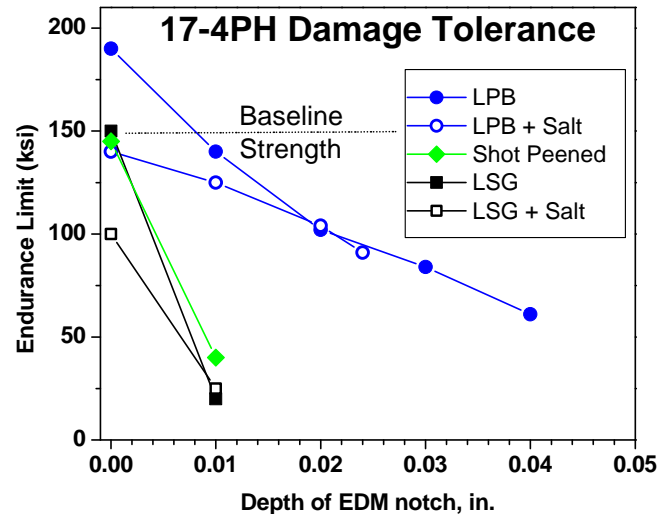


Figure 7: Fatigue strength of 17-4 PH SS - H1100 as a function of EDM notch depth for LSG, SP and LPB.

17-4PH Fractography

Optical fractography of the unnotched 17-4PH LSG, SP and LPB fracture surfaces tested in air indicated surface initiation in all cases, often from multiple origins as seen in Figure 9 for the SP sample. In active corrosion fatigue crack growth was intergranular, often originating from small surface corrosion pits, as shown in Figure 10 for LPB. All EDM notched samples failed from the bottom of the notch, as shown in Figure 11 for LPB where the depth of the compressive layer is indicated to scale.

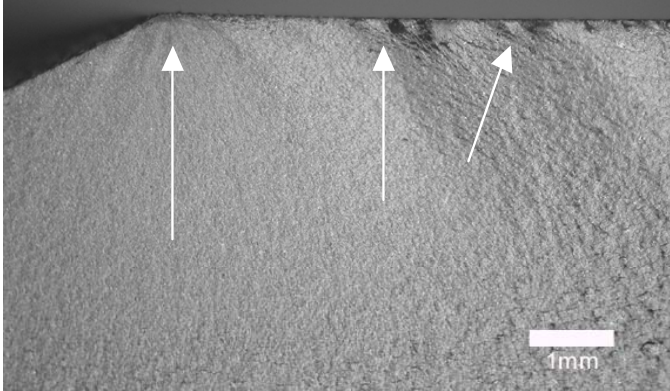


Figure 9: 17-4PH SP fracture, arrows indicate multiple crack initiation sites, $S_{max} = 181$ ksi (1,250 MPa), $N_f = 119,245$

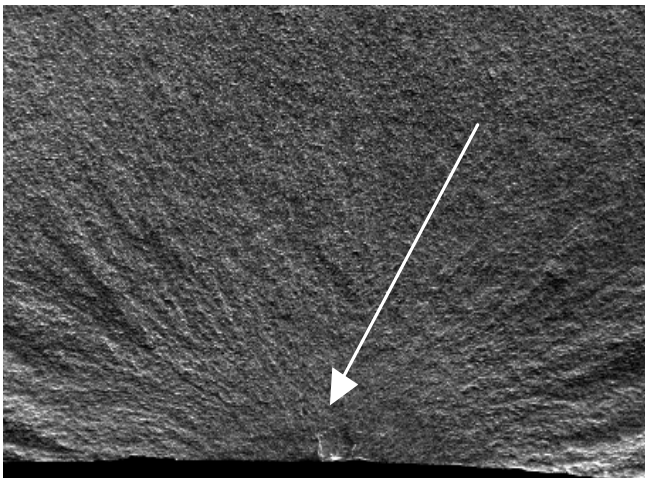


Figure 10: 17-4PH LPB + Salt unnotched fracture, arrow indicates origin, $S_{max} = 150$ ksi (1,035 MPa), $N_f = 316,613$

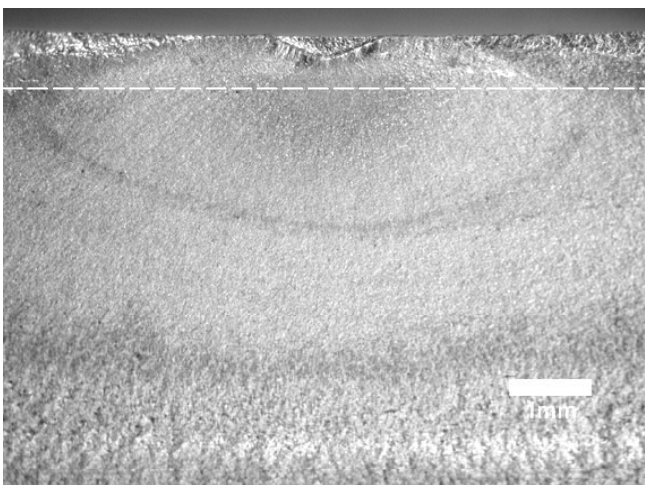


Figure 11: LPB + Salt + EDM notch (0.010 in.) fracture
Dotted line indicates the depth of compression.
 $S_{max} = 140$ ksi (965 MPa); $N_f = 794,917$

Alloy 450 Damage Tolerance and Corrosion Fatigue Performance

The corrosion fatigue performance of Alloy 450 stainless steel (H1050) tested in acidic NaCl solution is shown in Figure 8. The LSG baseline condition is compared with LPB with and without the EDM notch. The baseline fatigue strength at 10^7 cycles is nominally 100 ksi (~700 MPa). The EDM notch 0.010 in. (0.25mm) deep decreases the corrosion fatigue strength to only about 10 ksi (~70 MPa). The fatigue lives at higher stresses show a corresponding decrease of over an order of magnitude.

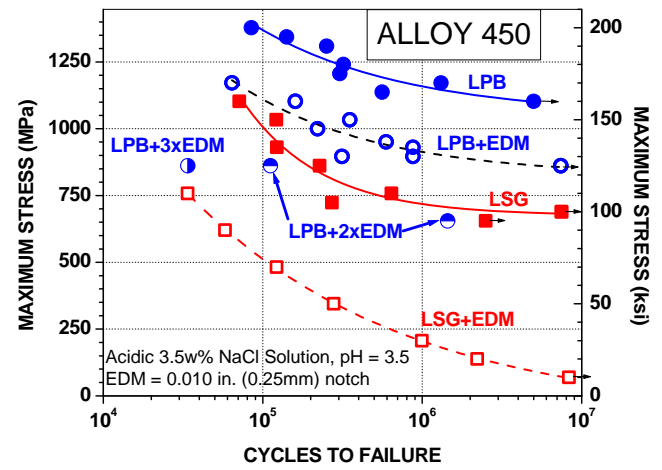


Figure 8. Alloy 450 Corrosion fatigue results for LSG and LPB surface treatments in acidic 3.5 wt% NaCl.

In contrast, unnotched LPB processed Alloy 450 has a fatigue strength of about 160 ksi (~1,100 MPa). The introduction of the EDM notch only marginally reduced the LPB fatigue strength to 125 ksi (860 MPa), well above the fatigue strength of the undamaged baseline specimens. To investigate the effects of deeper damage, two LPB specimens were tested with 0.020 in. (0.5 mm) deep EDM notches at 120 ksi (~825 MPa) and 95 ksi (~655 MPa). LPB with the 2x deeper damage gave fatigue lives comparable to undamaged LSG specimens, within the limits of experimental scatter. However, the LPB specimen with an EDM notch 3x deep tested at 120 ksi (~825 MPa) showed a substantial decrease in fatigue life, indicating that the notch effectively penetrated the layer of LPB compression shown in Figure 3.

Alloy 450 Fractography

Optical and SEM fractography indicated multiple surface initiation on the unnotched LSG Alloy 450 samples. Because all Alloy 450 samples were tested in an acidic salt solution, fatigue generally initiated from small surface corrosion pits. The crack growth was primarily

intergranular in all specimens, independent of surface treatment.

Crack initiation in the Alloy 450 LPB samples was subsurface, as seen in Figure 12, indicating that the compressive residual stress from the LPB treatment was prevented crack initiation from the surface pits. The typical notched LPB fracture face in Figure 13 shows the dark coloration beneath the notch, similar to that seen in Figure 12, attributed to corrosion on the crack surface. The radial crack growth marks converge at a point below the notch indicating subsurface initiation.

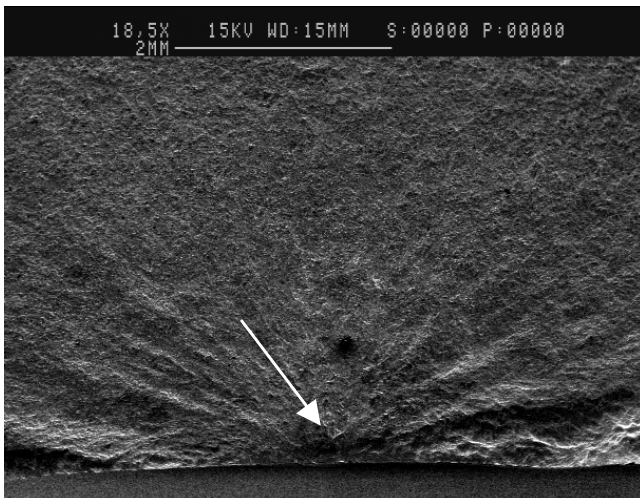


Figure 12: Subsurface origin on LPB Alloy 450, 0.5 mm from the surface, below the compressive layer, $S_{max} = 170$ ksi ($\sim 1,170$ MPa), $N_f = 1,311,786$

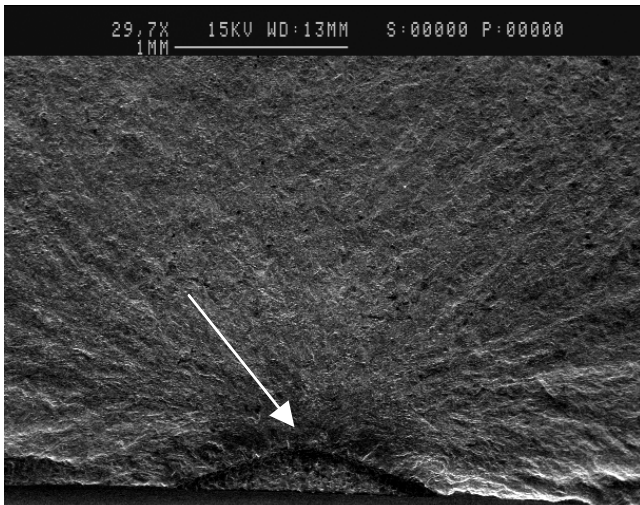


Figure 13: Subsurface initiation below EDM notch in LPB Alloy 450, $S_{max} = 135$ ksi (930 MPa), $N_f = 875,204$

DISCUSSION

Application of LPB to mitigate gas turbine compressor blade FOD³⁰ and dovetail fretting³¹ has been described in detail previously, including the caliper style tool shown in Figure 14. The caliper tool uses a patented constant volume hydrostatic bearing design to apply balanced forces simultaneously to both sides of the thin blade airfoil to develop through-thickness compression in the blade edge or tip. Variations of this caliper design have been developed for a range of blades ranging from meter-long low pressure steam turbine blades and small compressor blades such as the 17-4PH blade shown in Figure 14.

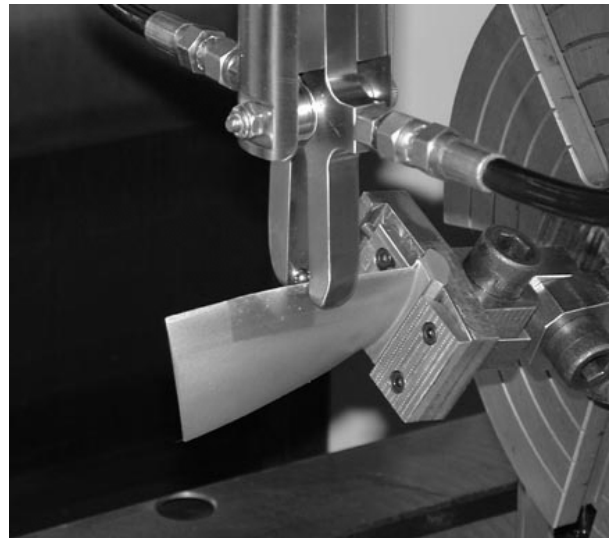


Figure 14: LPB caliper tool processing a thin 17-4 PH blade with equal force applied to both sides using paired patented constant volume hydrostatic supported burnishing balls

The depth of compression achievable with LPB exceeds that of conventional shot peening. An extreme Almen C range peening intensity using large balls would be needed to produce compression to 1 mm. With sufficient force and tooling, LPB has produced over 10 mm of compression. Shot peening dimples produce a rough surface that increases friction adversely impacting fluid flow at the blade surface, and may require remachining or polishing to restore the blade surface. LPB produces the highly polished surface of the ball tool embossed on the work piece while avoiding the highly cold worked roughened surface of shot peening.

The layer of surface compression is most effective in mitigating damage, such as erosion and corrosion pits, in high mean stress conditions encountered in stream turbine blade service. Consider the fatigue design diagram³² for 17-4PH shown in Figure 15. The blue curves labeled $k_f=1$ and $k_f=3$ are Smith-Watson-Topper¹ fatigue curves for a 10^7 cycle life without damage and with erosion, pitting, or other

damage that would reduce the fatigue strength to 1/3 of the baseline. The allowed alternating stress is adjusted for the damage using Neuber's rule¹. Any combination of mean and alternating stress above the blue lines will result in failure in less than 10^7 cycles.

A low pressure steam turbine blade may operate at a high mean stress of say 90 ksi. (Actual design stresses would, of course, be perhaps a third of this example for a 10^7 cycle life.) The maximum allowed alternating stress for an undamaged blade is nominally $S_{alt} = 60$ ksi, at point A in Figure 15. Placing the surface -100 ksi in compression, as in Figure 2, increases the allowed alternating stress at the surface to 90 ksi, point B. With $k_f = 3$ damage, the allowed alternating stress is reduced to only 10 ksi, point C in Figure 15. A layer of -100ksi compression deeper than the damage, such that the crack initiation point is held in residual compression, moves the surface and damage operating point to D, and the allowed alternating stress is increased to over 30 ksi, a 3-fold improvement for the damaged blade.

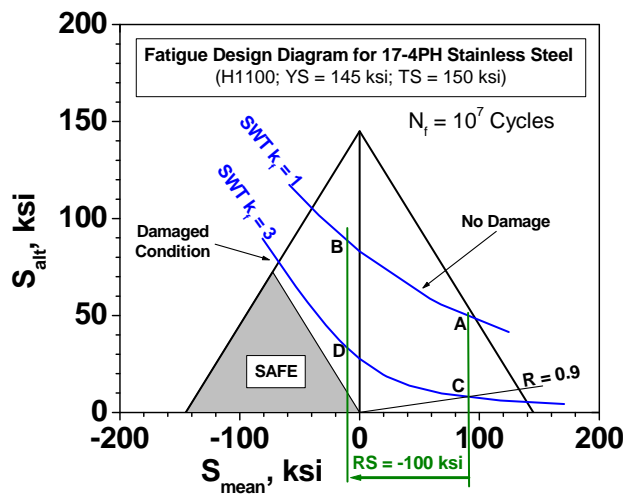


Figure 15: Fatigue Design Diagram for 17-4PH stainless steel showing the mean and alternating stress allowed for damaged and undamaged material and the benefit to introducing residual compression of -100 ksi.

Because the loading is elastic, that is confined within the triangle for the Haigh diagram forming the basis of Figure 15, the residual compression from LPB is not altered by cyclic loading in tension. No relaxation is observed unless the surface is loaded in compression so that the sum of the residual and applied compression exceeds the yield at the surface. The compressive surface is, of course, even less likely to yield in tension than the untreated material. Stability of LPB compression in cyclic loading has been repeatedly documented by residual stress measurement before and after fatigue testing to failure, and the additional

thermal stability due to low cold working of the surface confirms its suitability for long term service.

SUMMARY AND CONCLUSIONS

17-4PH

The 17-4PH stainless steel (H1100) damage tolerance and neutral salt solution corrosion fatigue performance are consistent with the subsurface residual stress distributions produced by the surface finishing treatments studied. For both LSG and shot peened specimens, the depth of compression is less than 0.010 in. (~ 0.25 mm), and damage on that order produces a comparable fatigue debit reducing the fatigue strength to only 25% of the baseline. The 0.040 in. (~ 1 mm) depth of LPB compression retards initiation and growth from either shallower damage or active corrosion, providing a fatigue strength nearly equal to undamaged 17-4PH tested in air. LPB mitigated the stress corrosion effects during cyclic loading, effectively restoring the endurance limit typically lost in corrosion fatigue.

Alloy 450

The corrosion fatigue and damage tolerance results for Alloy 450 (H1050) cycled in an acidic salt environment are also explained by the residual stress distributions produced by the surface treatments. In previous studies it is generally found that the fatigue strength of surface treated parts is approximately the same as the compressive residual stress at the initiation site. The surface residual stresses of -140 ksi (-965 MPa) and -175 ksi (-1,200 MPa) for the LPB treated specimens correlate quite well with the fatigue strength of LPB treated (unnotched) specimens at a value of about 160 ksi (~1,100 MPa). The residual stress at the notch depth of 0.010 in. (0.25 mm) is nominally 120 ksi (~825 MPa), on the order of the corrosion fatigue strength. The relation between the compressive stress at the depth of the 2x and 3x deep notches and the corresponding fatigue strength holds for the 2x and 3x deep notches.

LPB imparted highly beneficial compressive residual stresses on the surface, sufficient to withstand pitting and/or surface damage up to a depth of nominally 0.020 in. (0.5 mm) from the surface. LPB provided a 50% increase in corrosion fatigue strength in the absence of surface damage, and a 12x increase in strength for 0.010 in. deep damage. The fatigue strength improvement is attributed to the depth and magnitude of surface compression for both alloys.

ACKNOWLEDGEMENTS

Support for portions of this work by NAVAIR SBIR contract N68335-02-C-0384 is gratefully acknowledged. Authors also wish to thank Doug Hornbach for his help

with residual stress measurements and Perry Mason for his help in conducting fatigue tests.

REFERENCES

1. Frost, N.E. Marsh, K.J. Pook, L.P., *Metal Fatigue*, Oxford University Press, 1974.
2. Fuchs, H.O. and Stephens, R.I., *Metal Fatigue In Engineering*, John Wiley & Sons, 1980.
3. Berns, H. and Weber, L., "Influence of Residual Stresses on Crack Growth," *Impact Surface Treatment*, edited by S.A. Meguid, Elsevier, 33-44, 1984.
4. Ferreira, J.A.M., Boorrego, L.F.P., and Costa, J.D.M., "Effects of Surface Treatments on the Fatigue of Notched Bend Specimens," *Fatigue, Fract. Engng. Mater., Struct.*, Vol. 19 No.1, pp 111-117, 1996.
5. Prev y, P.S. Telesman, J. Gabb, T. and Kantzos, P., "FOD Resistance and Fatigue Crack Arrest in Low Plasticity Burnished IN718", *Proc of the 5th National High Cycle Fatigue Conference*, Chandler, AZ. March 7-9, 2000.
6. Clauer, A.H., "Laser Shock Peening for Fatigue Resistance," *Surface Performance of Titanium*, J.K. Gregory, et al, Editors, TMS Warrendale, PA (1996), pp 217-230.
7. T. Watanabe, K. Hattori, et al, "Effect of Ultrasonic Shot Peening on Fatigue Strength of High Strength Steel," *Proc. ICSP8*, Garmisch-Partenkirchen, Germany, Ed. L. Wagner, pg 305-310, 2002.
8. Paul S. Prevey, "The Effect of Cold Work on the Thermal Stability of Residual Compression in Surface Enhanced IN718", *Proceedings of the 20th ASM Materials Solutions Conference & Exposition*, St. Louis, MO, Oct. 10-12, 2000.
9. F. J. Heyman, V. P. Swaminathan, J.W. Cunningham, "Steam Turbine Blades: Considerations in Design and a Survey of Blade Failure," *EPRI Repot CS-1967*, Palo Alto, CA, EPRI, 1981.
10. C.S. Carter, D.G. Warwick, A.M. Ross, J.M. Uchida, *Corrosion*, 27, 1971, p190.
11. R.M. Thompson, G.B. Kohut, D.R. Candfield, W.R. Bass, *Corrosion*, 47, 1991, p216.
12. V.P. Swaminathan, J.W. Cunningham, *Corrosion Fatigue of Steam Turbine Blade Materials*, ed., R.I. Jaffee, Pergamon Press, New York, NY, 1983, p.3.1
13. P. Prev y, N. Jayaraman, R. Ravindranath, "Effect of Surface Treatments on HCF Performance and FOD Tolerance of a Ti-6Al-4V Vane," *Proceedings 8th National Turbine Engine HCF Conference*, Monterey, CA, April 14-16, 2003
14. Paul S. Prev y, Doug Hornbach, Terry Jacobs, and Ravi Ravindranath, "Improved Damage Tolerance in Titanium Alloy Fan Blades with Low Plasticity Burnishing," *Proceedings of the ASM IFHTSE Conference*, Columbus, OH, Oct. 7-10, 2002
15. Paul S. Prev y, et. al., "The Effect of Low Plasticity Burnishing (LPB) on the HCF Performance and FOD Resistance of Ti-6Al-4V," *Proceedings: 6th National Turbine Engine High Cycle Fatigue (HCF) Conference*, Jacksonville, FL, March 5-8, 2001.
16. M. Shepard, P. Prev y, N. Jayaraman, "Effect of Surface Treatments on Fretting Fatigue Performance of Ti-6Al-4V," *Proceedings 8th National Turbine Engine HCF Conference*, Monterey, CA, April 14-16, 2003
17. Paul S. Prev y and John T. Cammett, "Restoring Fatigue Performance of Corrosion Damaged AA7075-T6 and Fretting in 4340 Steel with Low Plasticity Burnishing," *Proceedings 6th Joint FAA/DoD/NASA Aging Aircraft Conference*, San Francisco, CA, Sept 16-19, 2002
18. N. Jayaraman, Paul S. Prev y, Murray Mahoney, "Fatigue Life Improvement of an Aluminum Alloy FSW with Low Plasticity Burnishing," *Proceedings 132nd TMS Annual Meeting*, San Diego, CA, Mar. 2-6, 2003.
19. Paul S. Prev y and John T. Cammett, "The Influence of Surface Enhancement by Low Plasticity Burnishing on the Corrosion Fatigue Performance of AA7075-T6," *Proceedings 5th International Aircraft Corrosion Workshop*, Solomons, Maryland, Aug. 20-23, 2002.
20. John T. Cammett and Paul S. Prev y, "Fatigue Strength Restoration in Corrosion Pitted 4340 Alloy Steel Via Low Plasticity Burnishing." Retrieved from www.lambda-research.com Sept. 5, 2003.
21. Paul S. Prev y, "Low Cost Corrosion Damage Mitigation and Improved Fatigue Performance of Low Plasticity Burnished 7075-T6", *Proceedings of the 4th International Aircraft Corrosion Workshop*, Solomons, MD, Aug. 22-25, 2000.
22. Hilley, M.E. ed., (2003), Residual Stress Measurement by X-Ray Diffraction, *HSJ784*, (Warrendale, PA: SAE).
23. Noyan, I.C. and Cohen, J.B., (1987) Residual Stress Measurement by Diffraction and Interpretation, (New York, NY: Springer-Verlag).
24. Cullity, B.D., (1978) Elements of X-ray Diffraction, 2nd ed., (Reading, MA: Addison-Wesley), pp. 447-476.
25. Prev y, P.S., (1986), "X-Ray Diffraction Residual Stress Techniques," *Metals Handbook*, **10**, (Metals Park, OH: ASM), pp 380-392.
26. Koistinen, D.P. and Marburger, R.E., (1964), Transactions of the ASM, **67**.
27. Moore, M.G. and Evans, W.P., (1958) "Mathematical Correction for Stress in Removed Layers in X-Ray Diffraction Residual Stress Analysis," *SAE Transactions*, **66**, pp. 340-345.
28. Prev y, P.S., (1986) "The Use of Pearson VII Functions in X-Ray Diffraction Residual Stress

- Measurement,” Adv. in X-Ray Analysis, Vol 29, (New York, NY: Plenum Press), pp 103-112.
29. Prev y, P.S., (1987), “The Measurement of Residual Stress and Cold Work Distributions in Nickel Base Alloys,” Residual Stress in Design, Process and Material Selection, (Metals Park, OH: ASM).
 30. P. Prevey, R. Ravendranath, M. Shepard, T. Gabb, “Case Studies of Fatigue Life Improvement Using Low Plasticity Burnishing in Gas Turbine Engine Applications,” Proceedings of ASME Turbo Expo, Atlanta, 2003.
 31. P. Prevey, N. Jayaraman, R. Ravendranath, M. Shepard, “mitigation of Fretting Fatigue Damage in Blades and Disk Pressure Faces with Low Plasticity Burnishing”, Proceedings of ASME Turbo Expo, Montreal 2007
 32. P. Prevey, N. Jayaraman and R. Ravindranath, “Introduction of Residual Stress to Enhance Fatigue Performance in the Initial Design”. Proceedings Turbo Expo 2004, Vienna, Austria, 2004.